https://doi.org/10.5194/egusphere-2026-4410
Preprint. Discussion started: 17 November 2026
© Author(s) 2026. CC BY 4.0 License.

Geomechanical insights into ice-wedge cracking from reanalysis-driven reinterpretation of legacy field studies

Gabriel Karam[1,2], Mehdi Pouragha[1], and Stephan Gruber[2]

[1]Department of Civil and Environmental Engineering, Carleton University, 1125 Colonel By Dr, Ottawa, ON, Canada
[2]Department of Geography and Environmental Studies, Carleton University, 1125 Colonel By Dr, Ottawa, ON, Canada

Correspondence: Gabriel Karam (gabrielkaram@cmail.carleton.ca)

Abstract.

We present a reanalysis-driven thermomechanical modeling framework that couples a degree-day snow boundary driving a Robin-type boundary with eXtended Finite Element Method (XFEM) fracture capability to reproduce legacy ice-wedge studies in permafrost. Soil layering and microtopography are incorporated to capture realistic field conditions in conjunction with downscaled and bias-corrected time series from atmospheric reanalysis. We simulated ice-wedge growth in newly forming epigenetic permafrost at drained lake Illisarvik (1978–1985) and the cracking of low-center polygons in Salluit (1989–1991). Calibration against available air and ground-surface temperatures showed good agreement using the degree-day snow boundary. Incorporating realistic soil layering reproduced the observed geometry of first-year cracks at Illisarvik, demonstrating the effects of stratigraphy on cracking. Microtopography at Salluit was shown to alter both the thermal regime and the stress field; counterintuitively, model configurations with a wider trough and greater snow accumulation were found to crack more frequently. Regarding the initiation and propagation direction of ice-wedge cracking, reducing wedge-ice tensile strength produced a shift in crack initiation location from the ground surface to the top of permafrost, offering an explanation for observed variations in crack directions due to variable ice properties. Microtopography and soil layering were both found to add a level of nuance that allowed the model to reproduce more complex aspects of ice-wedge cracking behavior and generate new knowledge.

1 Introduction

Ice wedges are widespread periglacial features in the continuous permafrost zone (e.g., Kokelj et al., 2014), forming signature polygons that cover millions of square kilometers. Their formation and growth are driven by thermal contraction cracking in cold permafrost: as temperatures decrease in winter, ground materials experience tensile stresses due to thermal contraction. When the tensile stress exceeds the strength of the ground, cracks form and propagate both vertically and laterally through the ground, intersecting to create polygonal networks. During spring snowmelt, water infiltrates these open cracks and freezes, forming successively larger ice bodies within the permafrost that can themselves crack during subsequent winters. Over repeated cycles, this process modifies the local microtopography and increases ground-ice content.

https://doi.org/10.5194/egusphere-2026-4410
Preprint. Discussion started: 17 November 2026
© Author(s) 2026. CC BY 4.0 License.

The contraction-cracking theory of ice-wedge formation was proposed by Leffingwell (1915) from field observations and later formalized by Lachenbruch (1962), whose analytical solution remains the most widely accepted numerical framework today. Numerous field studies have since expanded our understanding of the dynamics of ice-wedge cracking, with notable longitudinal studies by Mackay (1986), Mackay (1992), and Matsuoka et al. (2018).

In the past 25 years, many ice wedges have experienced degradation due to climate warming (e.g., Gagnon and Allard, 2020; Jorgenson et al., 2022; Liljedahl et al., 2016), increasing the release of greenhouse gases via thermokarst processes, and creating hazards that affect both the natural and the built environment. Understanding and quantifying how climate and local geology together determine ice-wedge evolution can help explain and model the patterns of ground-ice distribution that underpin thermokarst.

More recently, advances in numerical modeling have led to an improved understanding of the thermal regime within mature ice wedges. For example, Abolt et al. (2018) used a surface energy-balance model to study the thermal microtopographic effects of polygon ridges and troughs, while Garayshin et al. (2019) employed a finite-element model to simulate heat fluxes in developed ice wedges. In our previous numerical study, we complemented similar thermal analyses with geomechanical considerations to develop 2-D eXtended Finite Element Method (XFEM) models to simulate epigenetic ice-wedge growth in preexisting permafrost (Karam et al., 2024). These simulations reproduced the salient aspects of how soil characteristics and thermal conditions control thermal contraction cracking and ice-wedge growth using broad site characterization.

In this study, we aim to further quantify the effects of site-specific climatological and geological factors on ice-wedge cracking behavior, and to strengthen the link between geomechanics and field geocryology by reproducing legacy field studies. In order to formulate and test new hypotheses on ice-wedge cracking, our thermomechanical model must be able to represent detailed site-specific climate, surface, and subsurface conditions so that results can be reconciled with field observations. With this in mind, our objectives are: (1) to implement a simple surface boundary condition driven by air temperature and precipitation to allow the model to be applied at any location, driven by global atmospheric reanalyses; (2) to enhance the geological site representation with discrete soil layering and micro-topography to realistically capture observed site conditions; and (3) to answer long-standing questions from field studies, namely the driving factors behind the unique geometry of first-year thermal contraction cracks, the initiation and propagation direction of cracking in established wedges, and the thermomechanical effects of trough-rim topography.

2 Methods

2.1 Simulation overview

We employed ABAQUS 2021 with XFEM as the main simulation environment. Figures A1 and A2 are examples of typical model domain geometries used in this study, with the top boundary being the ground surface. Figure 1 schematically illustrates the 2-D plane broadly represented by the model, and the way in which individual wedges intersect the model plane.

In ABAQUS, we adopted a sequential modeling workflow in which air temperature and precipitation reanalysis data are used to drive a thermal model, whose output drives a mechanical model that captures the cracking process.

https://doi.org/10.5194/egusphere-2026-4410
Preprint. Discussion started: 17 November 2026
© Author(s) 2026. CC BY 4.0 License.

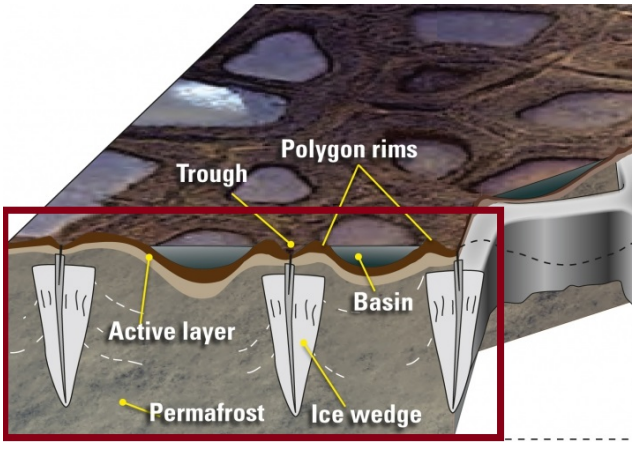


Figure 1. An illustration of low-centered ice-wedge polygons within the landscape, adapted from Martin et al. (2009), to show the transect of the 2-D model plane (red rectangle) within a 3-D volume. The model simulates both the active layer and permafrost layers and can also include preexisting ice wedges and soil layering, but is not equipped to include ponding or the movement of water.

In the thermal model, snow water equivalent (SWE) is estimated using a degree-day approach (Hock, 2003) and translated into a time-varying winter heat-transfer coefficient representing snow insulation during the winter. In the absence of snow, a fixed heat-transfer coefficient is applied (see Brown and Gruber, 2026; Tubini and Gruber, 2025).

Following the completion of the thermal simulation, the mechanical model received the resulting continuous time-series of the temperature field, used to calculate strains and stresses driven by the coefficient of thermal expansion and other mechanical properties of the ground material. Here, the condition for cracking is for the tensile stress to exceed the soil tensile strength, with crack initiation and propagation determined directly by the XFEM method. In this workflow, each pair of thermal and mechanical simulations covers one year of real time, so stress and temperature fields were transferred between subsequent years to ensure continuity.

2.2 Temperature-dependent material characteristics

Below °C, the ratio of frozen to unfrozen pore water in soils varies with temperature, leading to strong temperature dependence of many thermal and mechanical properties. We approximated these temperature dependencies using soil freezing characteristic curves calculated from the corresponding grain size distributions. Here, we assumed that soil is saturated and that there is no pore water movement. Five different typical ground materials were used: Suffield clay, Hanover silt, Manchester fine sand, Ottawa sand, and pure ice. These materials represent a spectrum of particle sizes from fine-grained clay to coarse sand and then pure ice. The temperature-dependent mechanical properties and mechanical constitutive models are described in Karam et al. (2024).

https://doi.org/10.5194/egusphere-2026-4410
Preprint. Discussion started: 17 November 2026
© Author(s) 2026. CC BY 4.0 License.

2.3 Driving weather data

Reanalysis air temperature and precipitation time series from ERA5 (Hersbach et al., 2020) and JRA-3Q (Kosaka et al., 2024) were used to drive the thermal model. These common data products, available globally starting in 1948, provide physically consistent sub-daily time series of weather data on a large global grid. From this grid, we performed downscaling using Globsim. Globsim allows large-scale reanalysis products to be interpolated to the point scale, providing input time series data for any location and available time period (Cao et al., 2019b).

After downscaling, remaining site-specific and broad-scale discrepancies (Cao et al., 2020; Cao and Gruber, 2025) were reduced using bias correction techniques (Cannon et al., 2020). We applied quantile mapping to correct downscaled reanalysis biases where site-specific air temperature observations were available. In this process, the relevant atmospheric data was split into training and test sets, then the quantile mapping adjustment was applied using the xclim Python package to produce a corrected output (Bourgault et al., 2023).

By using reanalysis data in combination with downscaling and bias correction, the potential applications of our model were expanded beyond the times and places with observed ground temperatures. This approach has previously been adopted in diverse applications and environments (e.g., Cao et al., 2017, 2019a; Fiddes and Gruber, 2014; Fiddes et al., 2015; Pozsgay and Gruber, 2025).

2.4 Surface boundary condition

A parsimonious boundary condition was used to represent the influence of air temperature, precipitation, and surface cover, with the approach detailed in Brown and Gruber (2026). SWE (SWE, mm) is used as a snowpack proxy; when SWE is above zero, a heat-transfer coefficient is applied at the top surface of the model ($\mathcal{H}_w$, in $\mathrm{W\,mm^{-2}\,K^{-1}}$). When no snow is present, the boundary prescribes a constant summer heat-transfer coefficient ($\mathcal{H}_s$, in $\mathrm{W\,mm^{-2}\,K^{-1}}$):

$$\mathcal{H} = \begin{cases} \mathcal{H}_w = min(\dfrac{1}{SWE\left(1-\dfrac{t}{\beta}\right)\gamma}, \mathcal{H}_s), & \text{for } SWE > 0 \\ \mathcal{H}_s, & \text{for } SWE = 0 \end{cases} \tag{1}$$

where γ ($\mathrm{W^{-1}\,mm\,K}$) converts SWE into an effective thermal resistance (R-value) and t (d, days) is the length of time the snowpack has been present. β (d, days) accounts for densification of the snowpack over time and was given a fixed value of 365. The change in SWE with time is determined using reanalysis precipitation and air temperature data, where:

$$\frac{d(SWE)}{dt} = \begin{cases} M_p\, M_{\text{veg}}\, M_{\text{top}}\, P, & \text{for } T < 2.8°C \\ M_p\, M_{\text{veg}}\, M_{\text{top}}\, P + M_{\text{melt}}\,(T_{\text{melt}} - T), & \text{for } 2.8°C > T \geq T_{\text{melt}} \\ M_{\text{melt}}\,(T_{\text{melt}} - T), & \text{for } T \geq T_{\text{melt}} \end{cases} \tag{2}$$

where P is the amount precipitation in $\mathrm{mm\,d^{-1}}$, T is the average daily temperature in $°C$, M_{top} is a modification factor to account for microtopography, and M_{veg} is a modification factor to account for changes in vegetation and its ability to trap snow.

https://doi.org/10.5194/egusphere-2026-4410
Preprint. Discussion started: 17 November 2026
© Author(s) 2026. CC BY 4.0 License.

M_p, M_{melt} ($\text{mm d}^{-1}\,\text{K}^{-1}$), and T_{melt} (°C) are additional calibration parameters. T_{melt} is always less than 0 °C such that both conditions in Eq. 2 can be true at the same time; this is for instances where precipitation falls in the form of snow even when near-surface air temperatures are above 0 °C. Depending on the exact temperature and amount of precipitation, this can result in either net accumulation or ablation at the ground surface.

To account for variations in snow accumulation due to microtopography, a factor M_{top} adjusts P before calculating SWE in Eq. 2. In a typical ice-wedge polygon, the ridges are windswept, resulting in a thinner snow layer, while the troughs accumulate deeper snow. Accordingly, the ridges and troughs are assigned factors of 0.3 and 1.75 respectively (e.g., Christiansen, 2005; Matsuoka et al., 2018), while the polygon flats remain unchanged with a factor of 1. The transition from ridge to trough was defined as piecewise, such that the M_{top} changes at predetermined points between the the polygon ridge, trough, and flat.

As part of the surface boundary condition, We also accounted for the effect of latent heat from the snowpack, which generally prevents ground surface temperatures from rising above 0 °C until the majority of the snow has melted. To represent this parsimoniously, an additional condition is included in the model boundary: if SWE is strictly positive and the boundary temperature is projected to exceed 0 °C during a timestep, the boundary is instead fixed at 0 °C for that timestep. This adjustment prevents the ground surface from warming unrealistically while preserving the evolution of the snowpack.

2.5 Calibration of the surface boundary condition

The model parameters introduced in Eqs. 1 and 2 were calibrated against observed ground-surface temperature (GST) series through a systematic trial-and-error process. The calibration procedure targets the five parameters in Table 1, using the specified value ranges. Nine representative parameter combinations were selected to balance calibration robustness and computational cost. The performance of these parameter sets in reproducing GST was evaluated based on the mean absolute error (MAE) and Pearson's coefficient (r), with the mean bias error (MBE) providing additional information. Using a rank-sum approach, the simulation with the lowest combined ranking of MAE and r was selected (Padilla-Ramirez, 2020). The choice of calibrated parameters is consistent with previously reported degree-day surface boundary conditions (e.g., Hock, 2003).

3 Experiments and field data

We developed two simulated experiments to reproduce the conditions of legacy field studies in Canada: the drained lake at Illisarvik, NT (69.4811°N, 134.5863°W) and a polygonal flat near Salluit, QC (62.1036°N, 75.7543°W). In both experiments, a simulated year begins on May 1st and ends on April 30th of the following calendar year, in order to avoid dividing the cracking process between two separate simulations.

3.1 Illisarvik 1978–1985

This simulated experiment explored the effect of soil layering on thermal contraction cracking by comparing multiple modeled subsurface configurations to field observations. Illisarvik is the drained basin of a thermokarst lake roughly 600 m long by 300 m wide, located on Richards Island, NWT (Mackay, 1986). It was artificially drained on August 13, 1978 for the express

https://doi.org/10.5194/egusphere-2026-4410
Preprint. Discussion started: 17 November 2026
© Author(s) 2026. CC BY 4.0 License.

Table 1. Calibration parameters modifying the thermal behavior of the surface boundary condition.

Parameter	Calibration range	Explanation
$\mathcal{H}_s$ ($\mathrm{W\,mm^{-2}\,K^{-1}}$)	$[1, 10]$	Summer heat-transfer coefficient
M_p	$[0, 1]$	Precipitation modifier
T_{melt} ($^\circ\mathrm{C}$)	$[-3, 0]$	Melt temperature
M_{melt} ($\mathrm{mm\,d^{-1}\,K^{-1}}$)	$[1, 4]$	Melt rate modifier
γ ($\mathrm{W^{-1}\,mm\,K}$)	$[0.12, 1.1]$	Proportionality coefficient

purpose of permafrost research. During the first two winters post-drainage, the bare lake bed experienced minimal snow accumulation and a polygonal network formed. In subsequent years, willows and shrubs began to grow noticeably around the residual pond by the summer of 1980, and vegetation slowly spread beyond the pond. This eventually led to increased snow depth, insulating the ground from the cold winter air and halting cracking events.

A typical cross-section of the drained lake was modeled as a 2-D rectangle, 40 m wide and 15 m deep, with gentle topographical variations to represent the lake bed. To simulate the talik and the change in thermal conditions caused by the drainage event, the entire model was kept at a constant 4 °C until the drainage date. After drainage, the surface boundary condition operated normally. To remain consistent with snow depth observations, M_{veg} was used to reduce the modeled SWE in the years immediately following drainage and increase it in subsequent years; M_{veg} was assigned a value between 0.05 to represent very limited vegetation and 1 to represent equilibrium vegetation growth. As there was no available site-specific GST data for Illisarvik at the time the simulation was run, the model was calibrated using 2017–2019 data from a nearby instrumented site (Pit 177, 69.2696°N, 132.9437°W; Ensom et al., 2020).

In Mackay (1986), the site stratigraphy was described as a 1–2 m layer of organic-rich silt overlying sand to depth. To test the effect of soil layering in the simulation, six configurations of Hanover silt and Ottawa sand were used, where C1 (Figure A2) matches the conditions observed in-situ most closely: C1 – 2 m of silt over 13 m of sand; C2 – 3 m of silt over 12 m of sand; C3 – 4 m of silt over 11 m of sand; C4 – 2 m of sand over 13 m of silt; C5 – 15 m silt; and C6 – 15 m sand. Here, each stratigraphic configuration is subjected to the same driving thermal data, whereupon results are recorded from 1978–1985.

3.2 Salluit 1989–1991

This simulated experiment explored the thermal and mechanical effects of the ridge and trough microtopography on thermal contraction cracking, as well as the hypothesis that ice strength can strongly influence the initiation location and direction of

https://doi.org/10.5194/egusphere-2026-4410
Preprint. Discussion started: 17 November 2026
© Author(s) 2026. CC BY 4.0 License.

crack propagation. Unlike the simulated Illisarvik, this experiment did not follow an observed pattern of real-world events, but rather used temperature and geometrical field measurements and did not attempt to reconcile cracking frequencies or timing. The aim here was to test the above hypotheses in ways that have not yet been directly applied in a field study.

The polygons at this site were classified as low-centered, with the soil in the troughs described as being 10 cm higher in elevation than the surrounding polygon flats, and the ridges rising 40 cm above the troughs (Allard and Kasper, 1998). The ground materials were noted to be comprised of a mix of fine sand layers overlying coarse fluvial deposits. In the absence of detailed material properties and soil core logs, we used the parameters for Manchester fine sand throughout the model domain. Based on drilling data from this study, wedge tops were located at an average depth of 30 cm below the trough surface and extended up to 6 m deep. Therefore, we set up the initial model geometry to include the existing ice wedges according to these measurements.

Three different plausible configurations of ridge and trough widths were used to explore the effect of microtopography (Figure A1): M1 – 0.8 m trough and 0.7 m ridges; M2 – 1.6 m trough and 1.4 m ridges; and M3 – 1.6 m trough and 0.7 m ridges. To quantify the differences produced by the three configurations, we recorded and summarized the thermal regime, stress regime, and cracking behavior for all three configurations from 1983–1991.

Apart from Mackay (1984), there has been little research into factors affecting the initiation location and direction of thermal contraction cracking. In studies such as Mackay and Burn (2002), it was noted that the ice in uncovered wedges can appear dirty, translucent, and contain air bubbles, which are factors can greatly affect the strength of ice (Jellinek, 1958; Lachenbruch, 1962). In order to investigate the influence of ice strength on crack initiation and propagation, we created two separate sets of simulations; one using the originally calibrated tensile strength of ice, and the second modifying the ice strength by a factor of 0.5.

Bias correction and calibration for Salluit used site-specific GST data from 2002–2005 (NordicanaD3, 2024). Reanalysis air temperature data from June 1, 1950 to May 31, 1975 was used to equilibrate the model with four spinup periods of 25 years and an initial model temperature of -5 $^{\circ}\mathrm{C}$. The temperatures in the spinup period represent a pre-climate warming state. After spinup, the model was run for the years 1975–1991 and compared with temperature observations for the winters of 1989–1990 and 1990–1991 from Allard and Kasper (1998).

4 Results

4.1 Illisarvik

4.1.1 Calibration

Figure 2 shows the performance of the selected calibration trial compared to GST observations, where good agreement is seen, particularly in capturing peak winter and summer temperatures. Some deviation can be seen at midwinter and melt-out, where the modeled temperatures showed a warm midwinter bias and cold melt-out bias.

https://doi.org/10.5194/egusphere-2026-4410
Preprint. Discussion started: 17 November 2026
© Author(s) 2026. CC BY 4.0 License.

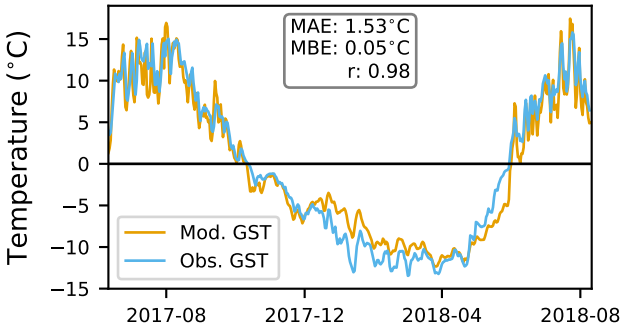


Figure 2. Comparison of calibrated and observed GST for Illisarvik, with observed GST obtained from Pit 177. The values for the calibration parameters were given as $\mathcal{H}_s = 10$, $M_p = 1$, $T_{\text{melt}} = -3$, $M_{\text{melt}} = 3$, $\gamma = 0.12$.

Table 2. Comparison of observed freezing and thawing degree days for Tuktoyaktuk from Mackay (1986) for the Tuktoyaktuk A weather station (Environment and Climate Change Canada, 2025) and the reanalysis data at Illisarvik. The top three rows are freezing degree days (FDD), and the bottom three are thawing degree days (TDD). TDD was not provided for 1978–1979 because lake drainage occurred in August.

Year	Metric	1978–1979	1979–1980
Mackay (1986)	FDD	4,525	8,850
TUK A	FDD	4,778	8,987
Reanalysis	FDD	4,453	8,614
Mackay (1986)	TDD	N/A	1,620
TUK A	TDD	791	1082
Reanalysis	TDD	694	950

4.1.2 Temperature measurements and permafrost aggradation

Following the lake drainage, Table 2 combines observations from the weather station at Tuktoyaktuk, NWT, Mackay (1986), and reanalysis data. It shows close agreement of modeled and observed freezing degree day values, but not of thawing degree day values. Mackay (1986) notes that the values are based on “air temperature data from Tuktoyaktuk”, but the TDD values recorded in the paper for 1979–1980 are much greater than the TDD we calculated from the historical weather station data and from the reanalysis data (Environment and Climate Change Canada, 2025).

Mackay (1986) measured permafrost aggradation with borehole temperatures and core samples. Comparatively, Fig. 3 shows considerable variation in the corresponding modeled results from different soil layering combinations, with the deviation appearing to be cumulative with time. Simulation results using C1 soil layering (thick brown lines) closely follow the bottom

https://doi.org/10.5194/egusphere-2026-4410
Preprint. Discussion started: 17 November 2026
© Author(s) 2026. CC BY 4.0 License.

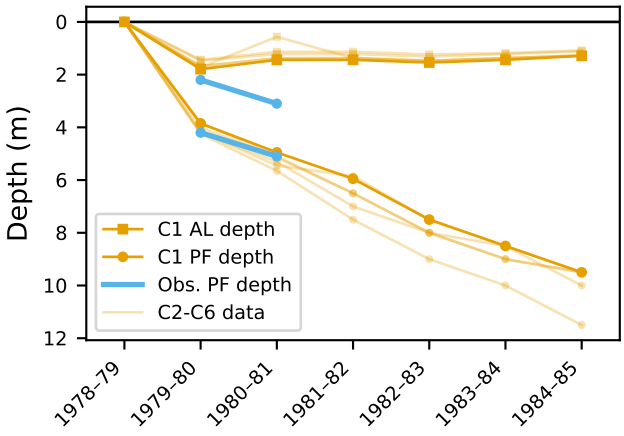


Figure 3. Evolving annual depths to the base of the simulated active layer and base of permafrost at Illisarvik. The opaque modeled lines are from C1 and the faint lines are from C2–C6. The blue lines for 1979 and 1980 indicate the measured values of the bottom of permafrost from Mackay (1986).

bound of observations (drill hole 79-1) while C2–C6 (thin brown lines) consistently overestimate permafrost depth. In contrast, there is less variation in active layer depth results between the different configurations; modeled results consistently showed the trend of a deeper initial active layer shallowing over time, which matches observations from Mackay and Burn (2002).

4.1.3 Geometry of first-year thermal contraction cracks

Mackay (1986) reports two separate crack width measurements: one set covers the first three years and is labeled maximum crack widths, whereas the second set covers the entire study period but no description is provided. Here, measurements from the second set are labeled as 'alternate'. In the absence of maximum cracking widths for the entire study period, we compare the modeled values against the maximum crack widths for the first three years and the alternate measurements for the entire study period. Figure 4 shows C1 is close in magnitude to the maximum widths where provided, and follows the decreasing trend with time of the alternate widths. When comparing C1 depth results to observations, there is agreement in both magnitude and trend. Similar to Fig. 3, there is considerable variation in the results for C2–C6.

Figure 5 further illustrates the contrasting simulated cracking geometries that developed from the different soil layering configurations used in the model. While the curved cracks seen in C3 and C4 do not match the field observations of cracks at Illisarvik, they bear resemblance to images from other exposed ice-wedge profiles (e.g., Leffingwell, 1915). Additional figures showing the development of the simulated ice-wedge cracks are provided in Appendix A: Fig. A4 presents multiple snapshots from the first year of cracking for C1 while Fig. A5 shows a single snapshot of each year of cracking layered model.

https://doi.org/10.5194/egusphere-2026-4410
Preprint. Discussion started: 17 November 2026
© Author(s) 2026. CC BY 4.0 License.

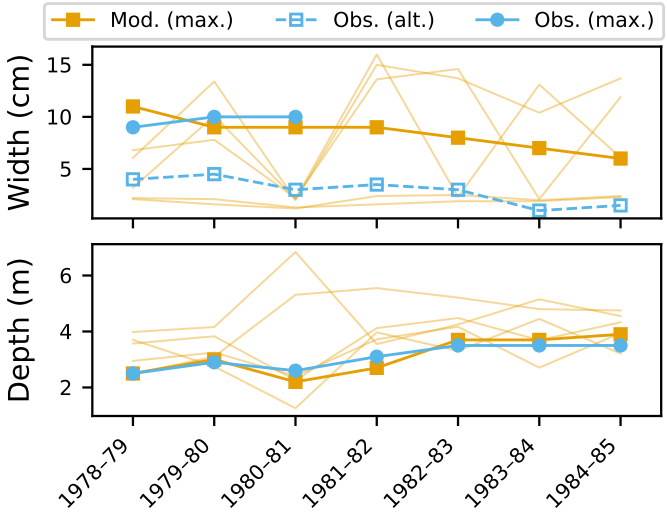


Figure 4. Comparison of observed and simulated crack geometry at Illisarvik. The opaque modeled lines are from C1 and the faint lines are from C2–C6. The field measurements were obtained using a 0.5 mm-thick steel surveyor tape to probe the depth and shape of the crack (Mackay, 1986).

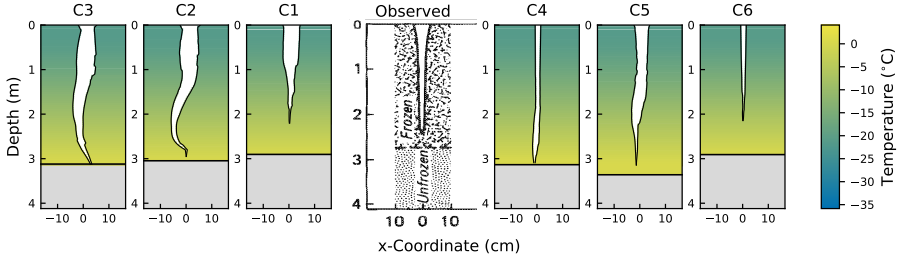


Figure 5. Simulated crack results using configurations C1–C6 from May 1, 1979, compared to a measured crack cross-section - Fig. 7 - from Mackay (1986). The gray area denotes unfrozen ground and the color map shows the temperature of the ground surrounding each crack.

4.2 Salluit

4.2.1 Calibration and thermal comparison

The selected calibration with configuration M1 shows good agreement with observed GST (Fig. 6) after the quantile mapping procedure reduced the air-temperature cold bias from -2.6°C to -0.2°C (Fig. A3). Some deviation occurs during the melt-out periods, particularly in winter 2004–2005, where observed temperature fluctuations are more pronounced than in the simulated GST time series.

https://doi.org/10.5194/egusphere-2026-4410
Preprint. Discussion started: 17 November 2026
© Author(s) 2026. CC BY 4.0 License.

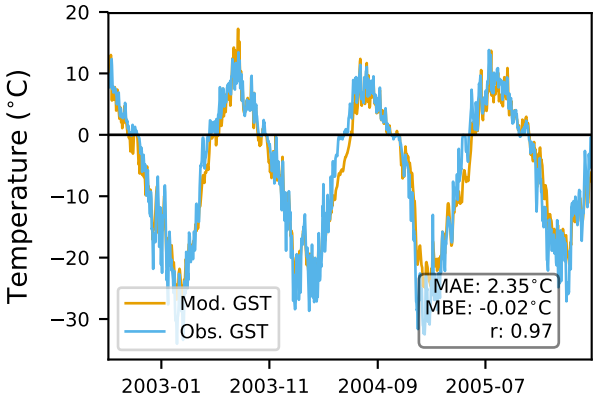


Figure 6. Comparison of modeled GST for Salluit using configuration M1, with observed data from NordicanaD3 (2024). The values for the calibration parameters were given as $\mathcal{H}_s = 10$, $M_p = 1$, $T_{\text{melt}} = -1$, $M_{\text{melt}} = 2$, $\gamma = 0.024$.

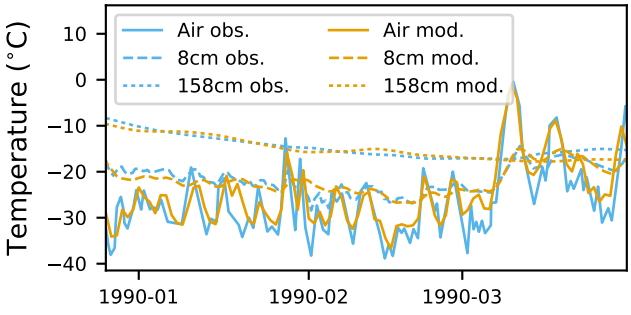


Figure 7. Comparison of simulated ground temperatures using configuration M1 against temperature observations from Allard and Kasper (1998).

Allard and Kasper (1998) provide temperature measurements at several depths with which we compare model results. Figure 7 highlights the match between observed and modeled temperatures at all three depths for which observational data were provided.

4.2.2 Stress and cracking geometry for different microtopographic configurations

For microtopographic configuration, we extracted temperature and stress values at two locations where cracking initiates: the ground surface at the bottom of the trough (GS) and the top of the wedge at the permafrost table (PT). Comparing the temperature plots for M1–M3 in Fig. 8 shows a temperature difference of roughly 1 °C at PT, though no clear trend is seen at GS. The larger trough and smaller ridges in configurations M2 and M3 reduced the cooling of the ground surface due to greater snow cover, leading to higher average temperatures. Figure 8 also shows that the differences in stress did not mirror the

https://doi.org/10.5194/egusphere-2026-4410
Preprint. Discussion started: 17 November 2026
© Author(s) 2026. CC BY 4.0 License.

differences in temperature at either location of interest. At GS, the average stress hierarchy for the 75th percentile was M1 > M2 > M3, and at PT it was M2 > M3 > M1. Varying stress results were recorded each year, with no apparent trend.

The lack of a monotonic relationship between temperature and stress could be potentially explained by the viscoelastic nature of the constitutive model. In a Maxwell-type formulation, thermally induced elastic stresses are continuously relaxed by viscous deformation, such that stresses at any given time depend not only on the instantaneous temperature but also on its preceding history. Because both elastic and viscous parameters are strongly temperature dependent, the resulting stress evolution exhibits a fading-memory behavior, which leads in turn to more complex dependencies between temperature history and stresses.

Examining the crack geometry (depth and width) in Fig. 8 shows that, for the nine years of simulated cracking, M3 had the highest average crack depth and width by a slim margin compared to M2, with M1 having had smaller overall volume of cracking compared to the other two configurations. M1 also cracked the least frequently, with four cracks in nine years, while M2 and M3 both cracked six times each over the study period. In Fig. 8, it should also be noted that stress at the wedge top was comparatively higher than stress at the bottom of the trough, despite having similar temperatures. This can be associated with the different thermal expansion coefficients of ice and soil (Lachenbruch, 1962), which likely led to a difference in strain for both materials and an increase in tensile stress on the ice side of the soil-ice interface.

4.2.3 Effect of ice strength on the direction of crack propagation

This section concerns the contrasting simulations in which only the tensile strength of the wedge ice was varied. In the simulations with the original ice strength, the majority of cracks initiated at GS and propagated downward. In contrast, when the ice strength was reduced, the majority of cracks initiated at PT and progressed upward to GS as well as downward through the wedge. No simulated cracks were found to have initiated at locations other than GS or PT.

5 Interpretation and discussion

5.1 Expanding the scope of model application through an improved surface boundary condition

The primary motivation for implementing a new boundary condition was to broaden the applicability of the model across a wider range of simulation scenarios through both time and space. Coupling this with reanalysis data allowed us to simulate sites that would otherwise be inaccessible to this or similar types of analyses due to missing or incomplete GST data. While long periods of observational data are ideal for thermal calibration, even a short or discontinuous GST record can be used to expand the scope of potential model applications.

The calibration results for Illisarvik and Salluit demonstrate the ability of the simple surface model to represent GST when used in conjunction with bias correction and other statistical methods. At both sites, the simple snow model captured winter temperatures and generally performed well, with two areas of reduced accuracy discussed below.

https://doi.org/10.5194/egusphere-2026-4410
Preprint. Discussion started: 17 November 2026
© Author(s) 2026. CC BY 4.0 License.

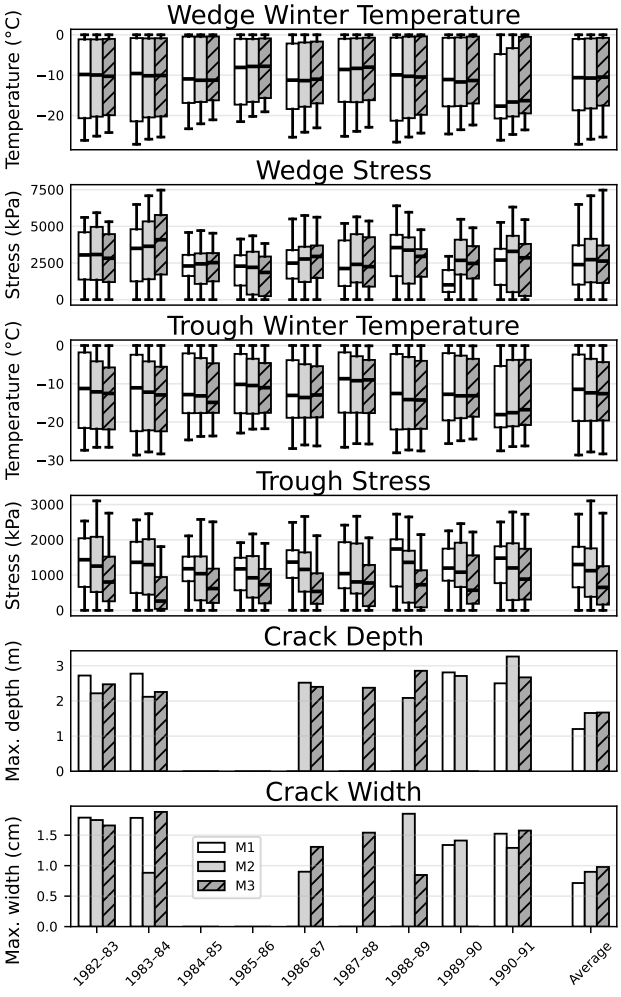


Figure 8. Comparison of winter temperatures, stress, and cracking geometry near the top of the Salluit ice wedge for the three microtopographic configurations M1–M3. The box plot whiskers indicate extreme values that are within 1.5 times the interquartile range.

First, ground warming in spring tended to be underrepresented; the simulated melt-out period where GST rises above 0 °C was consistently later than its observed counterpart. This was likely due to the simplifying assumptions of the model: in reality, solar radiation and meltwater percolation can quickly warm the ground in ways that are not captured by air temperature and a heat-transfer coefficient alone. Second, simulated winter temperature fluctuations were found to be weaker than observations, likely because the linear r-value calibration metric is less sensitive to the magnitude of fluctuations than the overall magnitude of error between the two datasets. Using an r-squared value may improve this shortcoming but could result in greater average differences.

https://doi.org/10.5194/egusphere-2026-4410
Preprint. Discussion started: 17 November 2026
© Author(s) 2026. CC BY 4.0 License.

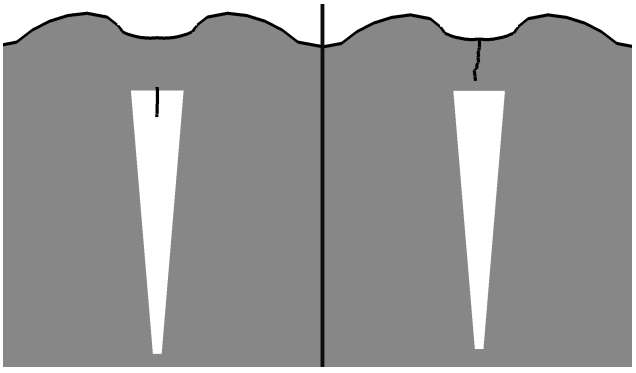


Figure 9. Simulated results showing differences in cracking initiation and propagation for Salluit between Jan 10 and 15, 1990. Left, ice strength was reduced by a factor of two and the crack initiated at PT, propagating both upward and downward. Right, ice strength was not altered, and the crack initiated at GS, propagating downward.

The critical period for capturing the thermal contraction cracking process is mid-winter when temperatures are at their lowest and most cracking occurs. Therefore, the under-representation of ground warming near melt-out is expected to be less consequential as cracking rarely takes place during warming periods. In contrast, the dampening of winter temperature fluctuations is more likely to influence the cracking process, though the comparison of crack depths and widths in this study showed good agreement despite this potential source of error.

5.2 Realistic subsurface representation leading to more accurate cracking results

At Illisarvik, the effect of soil layering was clear when comparing the six configurations: the model that most accurately portrayed the observed ground conditions was also better at replicating the observed permafrost depths, crack depths, and crack widths. The C1 crack shape as well as its long-term trends in geometry also showed considerably better agreement with field observations than any of the other configurations.

Figure 10 shows separate field evidence of the effect of soil layering on cracking; the relict wedge profile is cut-off at the boundary between an upper layer of fine organic-rich soil and a lower coarse layer dominated by gravel and boulders. The ice veinlet shows that cracks were sometimes able to propagate into the coarse layer, likely in exceptionally cold winters, but they did not progress far and reopened very infrequently. The clear visual effect produced by the difference in soil type provides an observational analogue to the varied simulated cracking results shown in Fig. 5.

5.3 A case for the evolution of first-year cracks in a drained lake basin

First-year thermal contraction cracks are unique and have been characterized in field studies by their large width and blunted bottom, features which are not shared by cracks in more developed wedges. In Mackay (1986), this was first observed when first-year cracks extended close to the bottom of permafrost. In the simulated results, similar features can be seen in Figs. 5

https://doi.org/10.5194/egusphere-2026-4410
Preprint. Discussion started: 17 November 2026
© Author(s) 2026. CC BY 4.0 License.



Figure 10. Relict wedge north of Dawson City, YT, measuring approximately 75 cm in height and 30 cm in width at the top. The main body appears to be located in fine-grained material with visible organics, while a small veinlet is observed to have progressed into underlying layer of coarser material with visible boulders.

and A4, particularly in the 1979-01-01 panel of A4. From the frozen soil parameters used in the model, we suspect that the nonlinear and temperature-dependent mechanical properties of warm permafrost allow for a much easier enlargement of a crack than those of cold permafrost. The values of elastic and shear moduli, as well as tensile strength, can be as much as five times less at -0.5 °C than at -10 °C. Because the soil at the bottom of an aggrading permafrost layer is close to 0 °C, tensile stresses were able to easily widen the crack tip. In more mature wedges, this widening is restrained by the higher stiffness and strength of cold permafrost. It is likely that only the unique thermal regime of newly-aggrading permafrost promotes these large crack widths: areas with cold, strong permafrost form thin, angular cracks, and areas with warm, weak permafrost generally cannot generate enough stress to cause thermal contraction cracking. Figure A5 shows a gradual deepening and narrowing of cracks as the permafrost temperature decreases, indicating that this progression has likely also occurred at Illisarvik.

5.4 Controls on the crack initiation and propagation direction in established wedges

Determining the driving environmental factors behind the location of crack initiation and the consequent direction of propagation has been a longstanding question. In developed polygons, there have been two observed locations for initiation, namely the top of the trough (ground surface, GS) and at the top of the existing wedge (top of permafrost, PT). Mackay (1984) noted

https://doi.org/10.5194/egusphere-2026-4410
Preprint. Discussion started: 17 November 2026
© Author(s) 2026. CC BY 4.0 License.

that roughly half of wedges always initiated at the GS, and half cracked at both GS and PT. However, the same wedges did not consistently crack at the same location in subsequent years, and different wedges within the same polygonal network also exhibited different trends. Mackay (1984) was not able to draw any statistically significant correlations between the direction of cracking and environmental factors with the available data.

Considering the lowest temperatures usually occur at GS, it would be intuitive to assume cracking should always initiate at this location since low temperatures are generally correlated with higher ground tensile stresses. However, crack initiation at PT is made possible because of the interface between soil and ice; thermal stresses are governed by constrained thermal strain rather than temperature alone. In the wedge–soil system, ice and soil have different thermal expansion and stiffness properties, such that their free thermal contractions during cooling are incompatible. Assuming ice and soil are strongly bonded and enforcing a displacement compatibility along the soil–ice interface generates misfit stresses, which can concentrate near the wedge top where geometry and constraint change rapidly. As a result, tensile stresses within the wedge at the permafrost table can exceed those at the ground surface, providing a mechanical basis for the two contrasting crack initiation locations, as shown in Fig. 9.

Within this stress regime, varying the ice tensile strength within our model led to clear differences in the cracking pattern between the two trials (Fig. 9), indicating that wedge-ice strength could be one of the controlling factors behind the direction of ice-wedge cracking. Variations in wedge-ice conditions are commonly observed in the field where bubbles, imperfections, and trapped particles from the formation process lead to differences in ice strength that are inconsistent from year to year. Crack initiation and propagation may also respond to seasonal and inter-annual variations in water content in the active layer above in the vicinity of the wedge, a phenomenon we did not investigate.

5.5 Examining the effect of microtopography beyond temperature control

At Salluit, the low-centered wedge microtopography was found to affect both the thermal and mechanical behavior of the model. As shown in Abolt et al. (2018) and Christiansen (2005), the difference in snow cover between the polygon flat, trough, and ridges leads to a thermal regime that is more spatially variable. Although the trough is heavily insulated by snow in the winter, the windswept ridges act as radiators to remove heat from the ground, leading to lower overall temperatures at PT. These differences in temperature have been directly correlated with cracking behavior using empirical rules, but the simulated temperature, stress, and cracking results indicate that the relationships between these variables are more complex than may have previously been thought.

Figure 8 highlights the temporal differences between temperature, stress, and cracking behavior for the three topographic configurations. As expected, there was a consistent difference in temperatures, which echoes finding by Abolt et al. (2018) who reported similar thermal trends at PT by varying the elevation of the ridges and trough instead of their width. From previous publications, we expected that the lower extreme temperatures produced by M1 would lead to consistently greater and more frequent cracking compared to M2 and M3 (e.g., Christiansen, 2005; Karam et al., 2024; Kokelj et al., 2007; Mackay, 1993). However, for the nine years of simulations, this was not the case. This can be potentially attributed to the multitude of ways temperature affects the stress regimes, stiffness, and strength in a temperature-dependent viscoelastic system.

https://doi.org/10.5194/egusphere-2026-4410
Preprint. Discussion started: 17 November 2026
© Author(s) 2026. CC BY 4.0 License.

First of all, the stress at the two initiation locations showed variations that did not follow thermal trends and resulted in different cracking behavior. While microtopography has previously been shown to affect the stress regime indirectly by modifying the thermal regime, it likely also directly affects stresses within the ground by the nature of its geometry. These effects are not consistent year-to-year, indicating that the interplay of rate and temperature-dependent material properties leads to complex cracking results that are difficult or impossible to predict using simple empirical rules based solely on temperature trends.

We still attempt to contextualize the microtopography results, this time with statistical field data. Mackay (1992) is the most comprehensive longitudinal field study on crack frequency and drivers, but noted no statistically significant difference between ice wedges with well-developed or insignificant ridges. There was, however, a significant normal relationship between crack frequency and trough width, with cracking frequency peaking at $\tilde{1}.25$ m wide. Comparing this with the trough widths for M1–M3 shows some agreement between the two results, as the wider trough configurations (M2, M3) had greater crack frequency compared to M1 which had narrower troughs. Overall, more specific experiments are required to elucidate the different effects of microtopography on temperature, stress, and cracking behavior.

6 Conclusions

This study aimed to advance the understanding of climatic and geological controls on thermal contraction cracking as they relate to ice-wedge formation and evolution. We implemented an improved surface boundary condition and included soil layering and topography to better represent field conditions in our simulated experiments based on legacy field studies.

By using a parsimonious degree-day snow model as the ground-surface boundary, we were able to drive the simulations using reanalysis air temperature and precipitation data. The boundary condition was able to capture the insulating effects of snow and spatial differences in snow cover due to variations in microtopography near the wedge.

Incorporating realistic and site-specific soil layering and topography improved the accuracy of the model in predicting crack geometry and growth, using only typical thermal and mechanical soil parameters. At Illisarvik, carefully capturing in-situ soil layering reproduced cracking observations almost exactly, while other plausible configurations were shown to overestimate permafrost and cracking depths, highlighting the effect of layering on both stress distribution and crack geometry. At Salluit, differences in microtopography affected both the thermal and stress regimes, causing wedges with wider troughs and higher average temperatures to crack more frequently, as has been noted in previous works. Unexpectedly, no clear link between temperature differences at the top of wedge or ground surface were found.

The two simulated experiments provided new insight into both first-year thermal contraction cracks in newly forming epigenetic permafrost and the direction of cracking in mature wedges. The unique geometry of first-year wedges is likely due to the rapid change in soil mechanical properties as aggrading permafrost experiences a steep vertical temperature gradient, leading to a blunted crack bottom and large width. In mature wedges, ice strength was found to be a controlling factor in the initiation and direction of cracking, with weaker wedge-ice cracking at PT and stronger wedge-ice cracking at GS. This appears to be a plausible explanation give the well-documented variations in ice-strength caused by impurities such as soil particles, salts, or air bubbles.

https://doi.org/10.5194/egusphere-2026-4410
Preprint. Discussion started: 17 November 2026
© Author(s) 2026. CC BY 4.0 License.

Overall, the combination of atmospheric reanalysis with ground-temperature and geomechanical simulation helped to reconcile field observations and theory. It allowed us to learn more from in-situ observations made at differing times and differing places that would otherwise not be possible to reproduce. This approach helps connect existing knowledge in diverse communities for informing action (Gruber et al., 2023), and further underscores the value of open data sharing (cf., Brown et al., 2024) in an academic field where in-situ data is sparse and expensive.

With the increasing reliability of such simulation approaches, we will be able to systematically study how differing ground materials and climate histories determine continental-scale patterns of ice-wedge characteristics and thereby support the mapping of potential ground-ice occurrence.

Code and data availability. The model configuration files, forcing time series, results, and scripts to reproduce the figures will be archived in Zenodo upon acceptance. During review, materials are available from the corresponding author upon reasonable request.

https://doi.org/10.5194/egusphere-2026-4410
Preprint. Discussion started: 17 November 2026
© Author(s) 2026. CC BY 4.0 License.

Appendix A

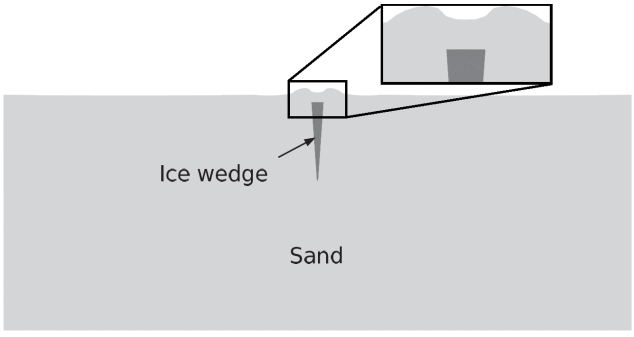


Figure A1. Model M1 used in the Salluit experiment showing a close-up of the wedge top and surface topography in the upper right-hand corner.

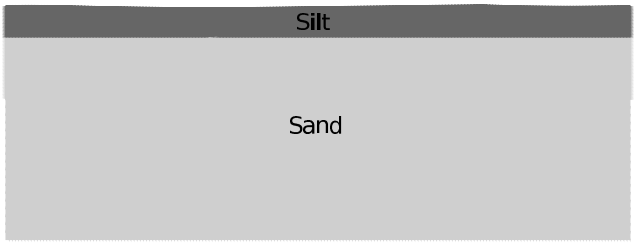


Figure A2. Model C1 used in the Illisarvik experiment, showing the silt-sand layering.

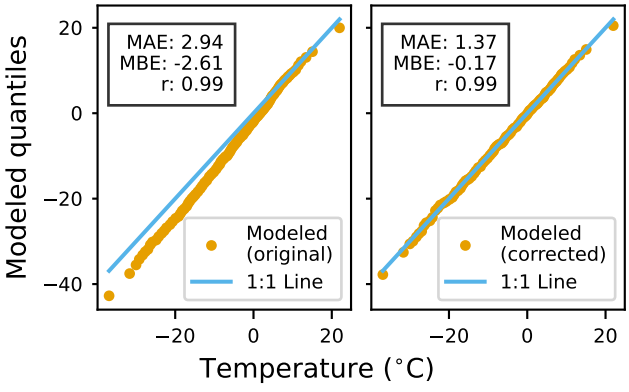


Figure A3. Quantile mapping results for ERA5 air temperature correction at Salluit.

https://doi.org/10.5194/egusphere-2026-4410
Preprint. Discussion started: 17 November 2026
© Author(s) 2026. CC BY 4.0 License.

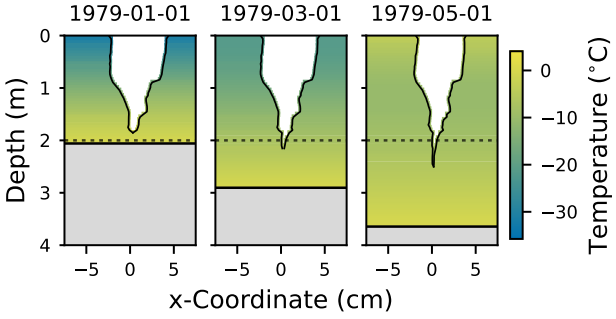


Figure A4. Snapshots of crack geometry and temperature for C1 at Illisarvik. The gray area denotes unfrozen ground and the dashed line denotes the boundary between silt (above) and sand (below).

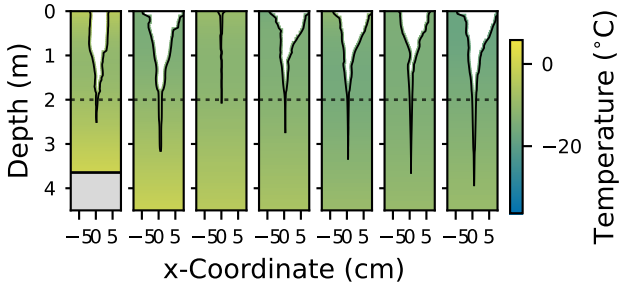


Figure A5. Comparison of modeled cracks from 1979–1985 on May 1st of each year. The gray area denotes unfrozen ground and the dashed line denotes the boundary between silt (above) and sand (below).

Author contributions. GK, MP, and SG conceptualized the study and developed the methodology; MP and SG contributed to funding acquisition, project administration, resources, and supervision; GK curated the data and performed the formal analysis using software; GK, MP, and SG performed validation and visualization; GK wrote the original manuscript draft; GK, MP, and SG reviewed and edited the manuscript.

Competing interests. The authors declare that they have no known competing financial interests or personal relationships that could have appeared to influence the work reported in this paper.

Acknowledgements. Funding was provided by the National Science and Engineering Research Council (NSERC) through the Strategic Partnership Network NSERC PermafrostNet (NETGP 523228-18) and Discovery Grant RGPIN-2020-04783.

https://doi.org/10.5194/egusphere-2026-4410
Preprint. Discussion started: 17 November 2026
© Author(s) 2026. CC BY 4.0 License.

References

Abolt, C. J., Young, M. H., Atchley, A. L., and Harp, D. R.: Microtopographic control on the ground thermal regime in ice wedge polygons, The Cryosphere, 12, 1957–1968, 2018.

Allard, M. and Kasper, J. N.: Temperature conditions for ice wedge cracking: field measurements from Salluit, northern Québec, in: Permafrost, Proceedings, 7th International Conference, Yellowknife, Canada, Centre d'etudes nordiques, Universite Laval, Collection Nordicana, vol. 57, pp. 5–11, 1998.

Bourgault, P., Huard, D., Smith, T. J., Logan, T., Aoun, A., Lavoie, J., Dupuis, É., Rondeau-Genesse, G., Alegre, R., Barnes, C., et al.: xclim: xarray-based climate data analytics, Journal of Open Source Software, 8, 5415, 2023.

Brown, N. and Gruber, S.: Beyond MAGT: learning more from permafrost thermal monitoring data with additional metrics, The Cryosphere, 20, 1771–1796, https://doi.org/10.5194/tc-20-1771-2026, 2026.

Brown, N., Gruber, S., Pulsifer, P., and Hayes, A.: A prototype field-to-publication data system for a multi-variable permafrost observation network, Environmental Modelling & Software, 175, 106 006, 2024.

Cannon, A. J., Piani, C., and Sippel, S.: Bias correction of climate model output for impact models, in: Climate extremes and their implications for impact and risk assessment, pp. 77–104, Elsevier, 2020.

Cao, B. and Gruber, S.: Brief communication: Reanalyses underperform in cold regions, raising concerns for climate services and research, EGUsphere [preprint], https://doi.org/10.5194/egusphere-2025-575, 2025.

Cao, B., Gruber, S., and Zhang, T.: REDCAPP (v1. 0): parameterizing valley inversions in air temperature data downscaled from reanalyses, Geoscientific Model Development, 10, 2905–2923, 2017.

Cao, B., Brown, N., Quan, X., Stewart-Jones, E., and Gruber, S.: Site-level permafrost simulation in remote areas driven by atmospheric reanalyses: a case study from the Northwest Territories, in: 18th International Conference on Cold Regions Engineering and 8th Canadian Permafrost Conference, pp. 534–543, American Society of Civil Engineers Reston, VA, 2019a.

Cao, B., Quan, X., Brown, N., Stewart-Jones, E., and Gruber, S.: GlobSim (v1. 0): deriving meteorological time series for point locations from multiple global reanalyses, Geoscientific Model Development, 12, 4661–4679, 2019b.

Cao, B., Gruber, S., Zheng, D., and Li, X.: The ERA5-Land soil temperature bias in permafrost regions, The Cryosphere, 14, 2581–2595, https://doi.org/10.5194/tc-14-2581-2020, 2020.

Christiansen, H. H.: Thermal regime of ice-wedge cracking in Adventdalen, Svalbard, Permafrost and Periglacial Processes, 16, 87–98, 2005.

Ensom, T., Kokelj, S., and McHugh, K.: Permafrost ground temperature report: Inuvik to Tuktoyaktuk Highway stream crossing and alignment sites, Northwest Territories, Northwest Territories Geological Survey (formerly Northwest Territories Geoscience Office and CS Lord Northern Geoscience Centre), 2020.

Environment and Climate Change Canada: Historical climate data for Tuktoyaktuk, https://climate.weather.gc.ca/index_e.html, extracted on July 10, 2025, 2025.

Fiddes, J. and Gruber, S.: TopoSCALE v. 1.0: downscaling gridded climate data in complex terrain, Geoscientific Model Development, 7, 387–405, 2014.

Fiddes, J., Endrizzi, S., and Gruber, S.: Large-area land surface simulations in heterogeneous terrain driven by global data sets: application to mountain permafrost, The Cryosphere, 9, 411–426, 2015.

Gagnon, S. and Allard, M.: Changes in ice-wedge activity over 25 years of climate change near Salluit, Nunavik (northern Québec, Canada), Permafrost and Periglacial Processes, 31, 69–84, 2020.

https://doi.org/10.5194/egusphere-2026-4410
Preprint. Discussion started: 17 November 2026
© Author(s) 2026. CC BY 4.0 License.

Garayshin, V., Nicolsky, D., and Romanovsky, V.: Numerical modeling of two-dimensional temperature field dynamics across non-deforming ice-wedge polygons, Cold Regions Science and Technology, 161, 115–128, 2019.

Gruber, S., Hayley, J., Karunaratne, K., King, J., MacLean, T., Marshall, S., and Moore, D.: Considerations toward a vision and strategy for permafrost knowledge in Canada, Arctic Science, 9, iv–viii, 2023.

Hersbach, H., Bell, B., Berrisford, P., Hirahara, S., Horányi, A., Muñoz-Sabater, J., Nicolas, J., Peubey, C., Radu, R., Schepers, D., et al.: The ERA5 global reanalysis, Quarterly Journal of the Royal Meteorological Society, 146, 1999–2049, 2020.

Hock, R.: Temperature index melt modelling in mountain areas, Journal of Hydrology, 282, 104–115, 2003.

Jellinek, H.: The influence of imperfections on the strength of ice, Proceedings of the Physical Society, 71, 797, 1958.

Jorgenson, M., Kanevskiy, M., Jorgenson, J., Liljedahl, A., Shur, Y., Epstein, H., Kent, K., Griffin, C., Daanen, R., Boldenow, M., et al.: Rapid transformation of tundra ecosystems from ice-wedge degradation, Global and Planetary Change, 216, 103 921, 2022.

Karam, G., Pouragha, M., and Gruber, S.: Investigating the controls of ice-wedge initiation and growth using XFEM, Computers and Geotechnics, 173, 106 549, 2024.

Kokelj, S., Pisaric, M., and Burn, C.: Cessation of ice-wedge development during the 20th century in spruce forests of eastern Mackenzie Delta, Northwest Territories, Canada, Canadian Journal of Earth Sciences, 44, 1503–1515, 2007.

Kokelj, S., Lantz, T., Wolfe, S., Kanigan, J., Morse, P., Coutts, R., Molina-Giraldo, N., and Burn, C.: Distribution and activity of ice wedges across the forest-tundra transition, western Arctic Canada, Journal of Geophysical Research: Earth Surface, 119, 2032–2047, 2014.

Kosaka, Y., Kobayashi, S., Harada, Y., Kobayashi, C., Naoe, H., Yoshimoto, K., Harada, M., Goto, N., Chiba, J., Miyaoka, K., et al.: The JRA-3Q reanalysis, Journal of the Meteorological Society of Japan. Ser. II, 102, 49–109, 2024.

Lachenbruch, A. H.: Mechanics of thermal contraction cracks and ice-wedge polygons in permafrost, vol. 70, Geological Society of America, 1962.

Leffingwell, E. d. K.: Ground-ice wedges: the dominant form of ground-ice on the north coast of Alaska, The Journal of Geology, 23, 635–654, 1915.

Liljedahl, A. K., Boike, J., Daanen, R. P., Fedorov, A. N., Frost, G. V., Grosse, G., Hinzman, L. D., Iijma, Y., Jorgenson, J. C., Matveyeva, N., et al.: Pan-Arctic ice-wedge degradation in warming permafrost and its influence on tundra hydrology, Nature Geoscience, 9, 312–318, 2016.

Mackay, J. R.: The direction of ice-wedge cracking in permafrost: downward or upward?, Canadian Journal of Earth Sciences, 21, 516–524, 1984.

Mackay, J. R.: The first 7 years (1978–1985) of ice wedge growth, Illisarvik experimental drained lake site, western Arctic coast, Canadian Journal of Earth Sciences, 23, 1782–1795, 1986.

Mackay, J. R.: The frequency of ice-wedge cracking (1967–1987) at Garry Island, Western Arctic coast, Canada, Canadian Journal of Earth Sciences, 29, 236–248, 1992.

Mackay, J. R.: Air temperature, snow cover, creep of frozen ground, and the time of ice-wedge cracking, western Arctic coast, Canadian Journal of Earth Sciences, 30, 1720–1729, 1993.

Mackay, J. R. and Burn, C.: The first 20 years (1978-1979 to 1998–1999) of ice-wedge growth at the Illisarvik experimental drained lake site, western Arctic coast, Canada, Canadian Journal of Earth Sciences, 39, 95–111, 2002.

Martin, P., Jenkins, J., Adams, F., Jorgenson, M., Matz, A., Payer, D., Reynolds, P., Tidwell, A., and Zelenak, J.: Wildlife response to environmental Arctic change (WildREACH): predicting future habitats of Arctic Alaska, Fairbanks, AK: US Fish and Wildlife Service, 2009.

https://doi.org/10.5194/egusphere-2026-4410
Preprint. Discussion started: 17 November 2026
© Author(s) 2026. CC BY 4.0 License.



Matsuoka, N., Christiansen, H. H., and Watanabe, T.: Ice-wedge polygon dynamics in Svalbard: lessons from a decade of automated multi-sensor monitoring, Permafrost and Periglacial Processes, 29, 210–227, 2018.

NordicanaD3: Climate station data from the Salluit Region in Nunavik, Quebec, Canada, CEN 2024, 2024.

Padilla-Ramirez, L. D.: Evaluating the effect of accordance measure choice on the selection of ground surface temperature models in a sub-Arctic environment, Ph.D. thesis, Carleton University, 2020.

Pozsgay, V. and Gruber, S.: Modelling the temporal dynamics of subarctic surface temperature inversions from atmospheric reanalysis for producing point-scale multi-decade meteorological time series in mountains, Arctic Science, 11, 2025.

Tubini, N. and Gruber, S.: Simulating soil heat transfer with excess ice, erosion and deposition, guaranteed energy conservation, adaptive mesh refinement, and accurate spin-up (FreeThawXice1D), The Cryosphere, https://doi.org/10.5194/egusphere-2025-2649, submitted, 2025.